Title

Cancer-associated arginine-to-histidine mutations confer a gain in pH sensing to mutant proteins.

Journal

Science signaling, 10(495)

ISSN

1945-0877

Authors

White, Katharine A
Ruiz, Diego Garrido
Szpiech, Zachary A
et al.

Publication Date

2017-09-01

DOI

10.1126/scisignal.aam9931

Peer reviewed

Arginine to Histidine Cancer Mutations Confer a Gain in pH Sensing to Mutant Proteins

Katharine A. White[1], Diego Garrido Ruiz[2], Zachary A. Szpiech[3], Nicolas B. Strauli[3], Ryan D. Hernandez[3,4,5], Matthew P. Jacobson[2], Diane L. Barber[1,*]

[1]Department of Cell and Tissue Biology, University of California, San Francisco.

[2]Department of Pharmaceutical Chemistry, University of California, San Francisco.

[3]Department of Bioengineering and Therapeutic Sciences, University of California, San Francisco.

[4]Quantitative Biosciences Institute, University of California, San Francisco.

[5]Institute for Human Genetics, University of California, San Francisco.

*Corresponding author
Diane L. Barber, PhD
Box 0512
University of California San Francisco
San Francisco, CA 94143
FAX: 415-502-7338
Email: diane.barber@ucsf.edu

Keywords: pH, cancer, EGFR, somatic mutation, p53

Summary: Arginine to histidine cancer mutations can confer a gain in pH sensing to mutant proteins, enabling tumorigenic phenotypes specifically at the higher intracellular pH of cancer cells.

ABSTRACT

The intracellular pH (pHi) of most cancers is constitutively higher than normal cells, enabling increased proliferation and cell survival. We show that increased pHi also enables tumorigenic behaviors through somatic arginine to histidine mutations, which are frequent in cancer and can confer pH-sensing not seen with wild-type proteins. We find that higher pH increases EGFR-R776H activity, causing increased cell proliferation and transformation. Molecular dynamics simulations suggest that changes in His776 protonation induce conformational changes in the αC helix. We also show that p53-R273H has decreased transcriptional activity and attenuated DNA damage response at higher pHi. Importantly, lowering pHi attenuates tumorigenic effects of both EGFR-R776H and p53-R273H. Our data suggest that some somatic mutations may confer a fitness advantage to the higher pHi of cancer cells.

INTRODUCTION

Increased pHi is an established feature of most cancers regardless of tissue or origin or genetic background (*1*). This increased pHi can enable tumorigenic properties such as increased proliferation, cell survival, and metastasis (*1-4*). Recent work suggests increased pHi may be both a cause and a consequence of tumor cell evolution (*5*). While the evolutionary theory of cancer has largely been shaped by genomic analysis of tumor samples (*6, 7*), cancer cell adaptation is mediated not by nucleotide changes but by proteomic changes that alter cell biology and enable cancer cell behaviors (White *et al*., JCS in press). Determining how distinct amino acid mutational signatures contribute to the physiological changes seen in cancer evolution is an understudied but important area of research. Recent work has analyzed cancers by amino acid substitution signatures (*8, 9*) and found that arginine to histidine (Arg>His) mutations are dominant in a subset of cancers. Anoosha and colleagues also showed that Arg>His mutations are enriched in driver over passenger mutations (*9*). The physiological implications of this Arg>His amino acid mutation signature has not been determined or proposed. Arg>His mutations are of particular interest given recent work on the molecular mechanisms of His switches in pH sensors, or proteins with pH sensitive functions or activities (*10*). Arginine with a pKa ~12 should always be protonated, while histidine with a pKa ~6.5 can titrate within the

narrow physiological pH range and exhibit a shift in population from the protonated to the neutral species at the higher pHi of cancer cells. With a gain in pH sensing, Arg>His substitutions could provide an adaptive advantage to cancer cells by altering protein binding or activity specifically at increased pHi.

Supporting this prediction, we tested two recurring Arg>His mutations in the epidermal growth factor receptor (EGFR-R776H) and p53 (p53-R273H). We selected these mutations because they are recurrent in human cancers (*11*), occur in functionally important regions of the proteins, and are candidates with predicted opposite effects with increased pHi—increase in EGFR enzyme activity and loss of p53 transcriptional activity. We and found that these Arg>His mutations confer pH sensing that is not seen with the wild-type proteins. We also present molecular mechanisms for how protonation changes at a single amino acid substitution can alter protein structure and activity of EGFR. We show that the adaptive pH sensing conferred by these Arg>His mutations enable cancer phenotypes specifically at increased pHi. Importantly, lowering pHi can effectively limit the tumorigenic effects of the Arg>His mutants. Our findings suggest that recent broad analyses of somatic amino acid substitutions in cancer can inform and direct studies of functional effects of somatic mutations at the protein level and, more importantly, may open new avenues for better classification and treatment of cancers.

RESULTS

EGFR-R776H has pH sensitive kinase activity *in vitro*.

We first tested our hypothesis that some Arg>His mutations can confer a gain in pH sensing by investigating by investigating a recurrent EGFR-R776H mutant (*11*). In the inactive crystal structure of wild-type EGFR (EGFR-WT) (*12*), Arg776 is involved in hydrogen bonding interactions with backbone carbonyl groups in the C-helix, which are not present in the active crystal structure (*13*) (Fig. 1A). Hence, structural data suggest that Arg776 may help stabilize the

inactive form of the kinase via this hydrogen-bonding network. Conformational reorganization of the αC helix is critical for kinase activity (*14*), and other activating EGFR mutations destabilize the inactive state (*15, 16*). We predicted that protonated His776 at lower pH might preserve the hydrogen-bonding network, while neutral His776 at higher pH would disrupt this network, causing a shift in the conformational equilibrium to active EGFR even in the absence of EGF.

We tested pH-dependent EGFR kinase activity *in vitro* using recombinant EGFR containing the intracellular kinase domain and juxtamembrane segments (residues 645-998) (*12*). Activity of EGFR-WT was pH insensitive, with similar levels of autophosphorylation and substrate phosphorylation at pH 7.5 compared to pH 6.8 (Fig. 1B, Fig. S1A). In contrast, EGFR-R776H activity was pH sensitive, with greater autophosphorylation and substrate phosphorylation at pH 7.5 than at pH 6.8 (Fig. 1B, Fig. S1A). Moreover, a pH titration revealed that EGFR-R776H was pH sensitive within a narrow pH range of 7.3 to 7.6 (Fig. S1B). These data suggest that the activity of EGFR-R776H is greater at the pHi of cancer cells (7.5-7.6) compared with the pH of normal cells (7.2). Additionally, the marked increase in EGFR-R776H activity within this range suggests that the pKa of His776 is upshifted compared to the pKa of histidine in solution (pKa 6.5).

EGFR-R776H confers increased pathway activation at higher pHi.

We confirmed pH-sensitive activity of EGFR-R776H when transiently expressed in EGFR-null MDA-MB-453 clonal breast cancer cells. Parental MDA-MB-453 cells have no response to EGF; but with transiently expressed recombinant EGFR-WT we observed an EGF-dependent increase in phosphorylated ERK (pERK) (Fig. S2A). We used 15-minute incubations with ammonium chloride (NH_4Cl) to increase pHi and 5-(N-ethyl-N-isopropyl) amiloride (EIPA), a selective inhibitor of the sodium proton exchanger NHE1, to decrease pHi (Fig. S2B).

While EGFR-WT activity was pH independent at the pH values we tested, EGFR-R776H was pH sensitive with increased activity at higher pHi (Fig. 1C). In the absence and presence of EGF, EGFR-R776H autophosphorylation (pY1173, Fig. 1C, D) and downstream phosphorylation of AKT (Fig. 1C, E) were greater at higher pHi. Moreover, in the absence of EGF, phosphorylation of AKT and ERK in cells expressing EGFR-R776H was greater at pHi 7.5 and greater than with EGFR-WT (Fig. 1E, F), indicating increased pathway activation at higher pHi in the absence of ligand. We also confirmed that EGFR-R776H had pH-dependent activity when expressed in another EGFR-null cell line (Chinese hamster ovary cells, Fig. S2C-D). To confirm that the pH-dependent activity observed in cells with EGFR-R776H is the result of titration at His776 and not due to the loss of Arg776, we tested a glycine substitution at position 776 (EGFR-R776G), which also occurs in human cancers (*11*). In contrast to EGFR-R776H, EGFR-R776G did not show pH-dependent activity under any condition tested (Fig. 1C-F). These data suggest that His776 specifically confers the pH-dependent activity observed with EGFR-R776H.

Molecular dynamics simulations reveal a mechanism for pH sensing by EGFR-R776H.

To identify a potential molecular mechanism for gain of pH sensing by EGFR-R776H, we used molecular dynamics (MD) simulations, an approach previously used to reveal EGFR transitions between active and inactive states (*17, 18*), regulatory mechanisms (*19*), and the impact of cancer mutations (*20*). A previous investigation of the activation mechanism of R776H in the EGFR kinase domain also focuses on the interactions around the αC – β4 loop, but does not take into consideration the effect of different possible protonation states for the mutant (*21*). Here, we explore the pH-dependent activation mechanism by explicitly comparing WT and both protonated and neutral R776H mutants.

We obtained 300 ns of molecular dynamics trajectories for EGFR-WT and EGFR-R776H with protonated and neutral His776. We performed the information theory-based Jensen-Shannon (JS) divergence analysis (*22*) to identify statistically significant differences in protein structure and dynamics for EGFR-R776H with protonated and neutral His776. We identified significant changes in structure and dynamics in the immediate vicinity of His776, as expected, but the largest JS divergence induced by changing the protonation state of His776 was localized around the αC helix N-terminal region (Fig. 2A), suggesting that protonation changes the conformational dynamics of the entire αC helix.

To characterize the αC helix conformation, we used two angle measures that quantify tilting and displacement of the helix relative to the conformation observed in the active crystal structure (Fig. 2B). We observed that the neutral His776 trajectory explored αC helix conformations that more closely resemble the active crystal structure than WT and protonated His776 (Fig. 2B). A superposition of final snapshots for each simulation shows the differences in conformations explored for WT and each protonation state of the R776H mutant (Fig. 2C). αC helix conformations sampled by neutral His776 (middle panel) were less constrained than those sampled by protonated His776 (right panel). WT αC helix conformations were also constrained near Arg776 (left panel), however the N-terminal region had more flexibility than protonated His776. In contrast, molecular dynamics simulations with EGFR-R776G showed that this mutant explored a wider range of αC helix conformations sampling both active- and inactive-like (Fig. S3). These data suggest that the protonation state of His776 can induce localized and dynamic conformational changes in a functionally critical region of EGFR.

EGFR-R776H enhances cancer phenotypes at higher pHi.

We also observed pH-dependent proliferation and transformation of cells expressing EGFR-R776H but not wild-type EGFR or EGFR-R776G. For these studies we stably expressed EGFR in NIH-3T3 cells (Fig. 3A) and experimentally changed pHi with NH_4Cl and EIPA as described above (Fig. 3B). We found that while proliferation of EGFR-WT and EGFR-R776G cells were comparable across tested pHi values, EGFR-R776H cells had greater proliferation at pHi 7.6 than at 7.2 (Fig. 3C). Consistent with previous findings that decreased pHi slows proliferation (*23*), proliferation of parental cells was lower at pHi 7.2 compared with 7.4; however, our findings suggest that expression of EGFR-WT, EGFR-R776G, or EGFR-R776H suppresses this effect. Additionally, transformation with EGFR-R776H, determined by colony formation in soft agar, was two-fold greater with increased pHi induced by NH_4Cl (Fig. 3D, E). In contrast, there was no transformation with EGFR-WT, and transformation with EGFR-R776G and oncogenic BRAF-V600E were both pH-independent. Taken together, these findings indicate that the dynamic pH sensitive activity of EGFR-R776H results in increased pathway activation, proliferation, and transformation at the higher pHi of cancer cells, which could confer an adaptive advantage to the cancer cells.

p53-R273H has pH sensitive transcriptional activity.

We showed with EGFR-R776H that increased pHi can enhance activity of an oncogenic mutation. To test the prediction that gain in pH sensing can suppress activity of a tumor suppressor at high pHi, we investigated p53-R273H, a highly recurrent somatic mutation in p53 (*24*). The co-crystal structure of p53 with DNA (*25*) suggests direct binding of positively charged Arg273 with the negatively charged phosphate backbone of DNA (Fig. 4A). We reasoned that protonated His273 could also form favorable electrostatic interactions with DNA but neutral His273 would not, thus conferring pH-sensitive DNA binding with decreased binding

at higher pHi. Although several studies have measured decreased DNA binding by p53-R273H (*26, 27*), to our knowledge pH-dependent binding and transcriptional activity have not been reported.

We used a luciferase reporter assay (*28*) to measure p53 transcriptional activity with experimentally changed pHi (Fig. S4A) in untransformed PS120 fibroblasts deficient in the sodium-proton exchanger NHE1 and that stably express an inactive NHE1-E266I mutant (*29, 30*). We transiently expressed WT or mutant p53 and induced a DNA damage response with etoposide. While transcriptional activity of p53-WT was pH insensitive, activity of p53-R273H was pH sensitive and decreased at higher pHi (Fig. 4B). In contrast, p53-R273L and p53-R175H both exhibited pH-independent and low transcriptional activity (Fig. 4B). These controls suggest that the pH-dependent transcriptional activity observed with p53-R273H is due to the titration of a histidine specifically located at the protein-DNA interface.

Cells expressing p53-R273H have pH sensitive transcriptional profile and survival.

Because PS120 fibroblasts have endogenous p53, we confirmed our findings on transcriptional activity using p53-null MDA-MB-157 clonal breast cancer cells stably expressing p53-WT or p53-R273H. We lowered pHi with an inhibitor of NHE1, 5-(N-ethyl-N-isopropyl) amiloride (EIPA), (Fig. S4B) and induced a DNA damage response with etoposide. Using an RT-PCR p53 profile array (Qiagen), we simultaneously quantified transcript levels for 83 members of the p53 signaling pathway at pHi 7.2 and 7.6. We found a pH-dependent transcriptional profile in cells expressing p53-R273H, with 20 transcripts differentially expressed at lower pHi in p53-R273H expressing cells (Fig. 4C). Nineteen transcripts, including pro-apoptotic or arrest transcripts such as ATM, BRCA1, CHEK1, and FADD, were more abundant at lower pHi in p53-R273H expressing cells and one pro-growth transcript, PTTG1, was less

abundant at lower pHi (Fig. S5). We also noted that a linear regression of 2^-ΔC(t) values for pHi 7.2 vs. pHi 7.6 gave a slope of 1.3 ($R^2 = 0.83$) for p53-R273H and 0.87 ($R^2 = 0.99$) for wild type p53. These data suggest that overall transcriptional activity of p53-R273H is decreased at higher pHi and that decreasing pHi can partially restore p53-R273H transcriptional activity of pro-apoptotic genes. At low pHi in cells expressing p53-R273H we observed transcript levels of CHEK1 and BRCA1 that are equivalent to that observed with p53-WT.

We also determined cell death in response to double strand breaks under conditions identical to the RT-PCR assay. We found that the p53-WT cell line exhibits pH-insensitive induction of cell death but p53-R273H has decreased cell death at increased pHi (Fig. 4D). Therefore, transcriptional activity and induction of cell death in response to DNA damage is decreased at higher pHi with p53-R273H, suggesting transcriptional activity of this mutant is attenuated at the higher pHi of cancer cells. Importantly, we were able to rescue functional p53-R273H response to double strand breaks by simply lowering pHi.

DISCUSSION

We find that p53-R273H and EGFR-R776H substitutions confer a gain in pH sensing not seen with wild-type protein, enabling cancer cell behaviors at higher pHi. These findings add to an emerging list of tumorigenic behaviors enabled by the established higher pHi of cancer cells. We previously described how the higher pHi of cancers increases cell proliferation and promotes hyperplasia and metastatic progression (*2, 4*). Our new findings suggest that increased pHi can work in concert with mutant proteins to limit tumor suppression and enhance oncogenic signaling. Moreover, lowering pHi attenuates some of the oncogenic effects of EGFR-R776H and partially restores p53-R273H tumor suppressor functions.

Despite findings on a higher than expected frequency of Arg>His mutations in cancer (*8, 9*), the functional or physiological relevance of recurring Arg>His substitutions has not been reported. Our data show that Arg>His mutations can confer a gain in pH sensing to mutant proteins and suggest that Arg>His substitutions may provide a fitness advantage to the increased pHi of cancer cells. This work provides the first analysis of potential physiological relevance of the higher than expected frequency of Arg>His mutations observed in cancer (*8, 9*). Furthermore, our functional cellular assays suggest that the tumorigenic effects of some somatic Arg>His cancer mutations become penetrant only at high pHi, and suggest that lowering pHi in cancer cells may reduce the deleterious effects of some Arg>His mutations. These findings lay the groundwork for future studies on the functional effects of other amino acid substitutions that may allow adaptive and advantageous responses to either altered pHi dynamics or dynamic microenvironment pressures in cancers such as oxidative stress, oxygen and nutrient availability, as well as metabolic reprogramming.

MATERIALS AND METHODS

EGFR activity. Cloning, expression, and *in vitro* activity assay details in Supplementary Methods. General cell culture conditions in Supplementary Methods. Cells were plated (1×10^5 per well; 6-well plate) and 24 h later transfected with 1 μg per well of pcDNA3-EGFR-WT (or EGFR-R776H, -R776G) using Lipofectamine 2000 (Invitrogen) according to mfg's protocol. 24 h post-transfection, medium changed to complete medium for 24 h and then cells were serum-starved for 24 h. *pHi control*. After serum-starvation, to raise pHi, cells were incubated with serum-free medium (SFM) containing 15 mM NH_4Cl for 10 min. To lower pHi, cells were incubated with SFM + 15 mM NH_4Cl for 10 min, then incubated with SFM + 1 μM EIPA for 5 min. Where indicated, cells were treated with EGF (50 ng/mL; 5 min) added to pH-control media. Cells were washed twice with ice-cold PBS and incubated with 100 μl of ice-cold lysis buffer (50 mM Tris, 150 mM NaCl, 1 mM NaF, 1% Triton X−100, protease inhibitor cocktail (Roche), pH 7.5) for 15 min on ice. Cells were scraped and clarified lysate (10,000 rpm; 10 min) was used immediately for western blotting or flash-frozen and stored at -80 °C. Western Blotting details in Supplementary Methods.

Molecular dynamics structure preparation. A complete structure for initiating molecular dynamics simulations was created using (2J6M) (*16*) and adding missing residues (R984-D1003) from another crystallographic structure (3POZ) (*31*). The two structures were aligned, missing residues were built in, and energy minimization performed on the composite model in PLOP (*32*). For histidine mutants with fixed protonation states, the Arg776 in the WT model structure file was mutated.

Molecular dynamics simulations. Amber's LEaP program was used with the Amber ff99SB force field and GAFF. The TIP3P water model was used to solvate the system in a cubic periodic box, such that the closest distance between any atom in the system and the periodic boundary is 10 Å. Net negative charge on EGFR was neutralized by adding counterions (Na+). Energy minimization was performed in two steps: using harmonic restraints on the protein (500.0 kcal mol^{-1} $Å^{-2}$) and an unrestrained minimization. For each step we ran 500 steps of steepest descent and 500 steps of conjugate gradient minimization at a constant volume with a non-bonded cutoff of 9 Å. The equilibration was done in three steps. First, the system was heated from 0 to 300 K with a restrained equilibration (10.0 kcal mol^{-1} $Å^{-2}$) for 20 ps at constant volume with a non-bonded cutoff of 9 Å, using the SHAKE algorithm to constrain bonds involving hydrogens, and the Andersen thermostat. The second round of equilibration was performed lowering the harmonic restraints (1.0 kcal mol^{-1} $Å^{-2}$) on the system for 20 ps (other parameters identical). The third round was performed for 10 ns at constant pressure of 1.0 bar with non-bonded cutoff of 9 Å at 300 K with the Andersen thermostat. Simulations were performed without restraints using new velocities with random seeds at constant pressure of 1 bar with non-bonded cutoff distance of 9 Å. Six independent 50 ns simulations were run with 2 fs timestep, for a total of 300 ns of simulation time per EGFR construct. Coordinates and energy were saved every picosecond (500 steps). Molecular dynamics simulation analysis details in Supplementary Methods.

Cell proliferation Stable cell line preparation in Supplementary Methods. NIH-3T3 parental or stable NIH-3T3 cell lines expressing EGFR-WT, -R776G, or -R776H were plated ($1×10^3$ per well; 24-well plate) in pHi control media (6 wells per condition). *pHi control*. Control: DMEM + 10% FBS. Increased pHi (NH_4Cl): DMEM + 10% FBS + 5 mM NH_4Cl. Decreased pHi (EIPA): DMEM + 10% FBS + 10 μM EIPA. 24 h and 72 h after plating, 3 wells of each condition were

trypsinized and living cells counted (Trypan blue exclusion). Proliferation reported as average fold-increase in cell number between 24 h and 72 h. Data analyzed from four experiments (one-way ANOVA, Tukey multiple comparisons correction).

Cell transformation Cells were plated on a solidified bed of 0.5% agarose in growth media in 3.5 cm plates. For plating, 1×10^4 3T3-EGFR-WT, 3T3-EGFR-R776G, 3T3-EGFR-R776H, or 3T3-BRAF-V600E stable cell lines were resuspended in 0.35% agarose in growth medium. Agar was topped with 2 mL of growth medium and incubated overnight. 24 h after plating, top medium was removed and replaced with pHi control medium. For BRAF plates, BRAF-V600E expression was induced (1 μM tamoxifen). *pHi control*. Control—DMEM + 10% FBS; NH_4Cl—DMEM + 10% FBS + 5 mM NH_4Cl. Medium was replaced every 3 days until day 15, when cells were washed twice in PBS, fixed with 4% PFA in PBS for 1 h, washed twice in PBS, and stained with 0.0005% crystal violet for 2 h. After PBS washes to remove excess crystal violet, images were acquired (Alpha Innotech FluorChem Q). Colonies were counted using Analyze Particles function on Image J software. Particles larger than 8 square pixels were quantified and averaged from two technical replicates per condition. This protocol was repeated for three biological replicates (Student's t-tests, unpaired, two-tailed, Holm-Sidak multiple comparisons correction).

Luciferase assay PS120 cells stably expressing NHE1-E266I (*29*) were plated (4×10^4 per well; 24-well plate). 24 h later, cells transfected (Lipofectamine 2000, Invitrogen) with 100 ng each of PG13-Luciferase (*28*) and pRK-β-galactosidase (control reporter) as well as 500 ng of p53 plasmid (pCB6-p53, p53-R175H, p53-R273L, or p53-R273H; wild-type plasmid provided by K. Vousden, Beaston Institute). Conditions with a non-specific reporter plasmid (MG13-Luciferase) (*28*) were used for background subtraction. *pHi control*. 24 h after transfection, pHi was altered.

To raise pHi: 5 mM NH_4Cl for 48 h. To lower pHi: 0.1 μM concanamycin A (Sigma, C9705), a V-ATPase inhibitor, for 48 h. To induce p53 response, 10 μM etoposide (Millipore, 341205) was added for the final 12 h. Luciferase and β-galactosidase activities were measured using Dual-Light Luciferase Assay (Roche) according to mfg instructions. Briefly, 10 μl of lysate was measured in duplicate for each condition and background-subtracted ratios of luciferase/β-galactosidase RLUs determined. Ratios were normalized within each experiment to that observed with p53-WT at low pHi. Data analyzed from 4 experiments (Student's t-tests, unpaired, two-tailed, Holm-Sidak multiple comparisons correction).

RT-PCR MDA-MB-157 cells stably expressing either wild-type p53 or p53-R273H were plated in 10 cm dishes and grown to ~50% confluency before beginning experimental modulation of pHi. *pHi control*. 24 h after transfection, pHi was altered. To raise pHi: medium supplemented with 5 mM NH_4Cl for 48 h. To lower pHi in MDA-MB-157: medium supplemented with 10 μM EIPA for 48 h. To induce a p53 response, 10 μM etoposide (Millipore, 341205) was added for the final 12 h. Cells were harvested and total RNA extracted using the RNAeasy Mini Kit (Qiagen). For each condition, 0.5 μg total RNA was used. Synthesis of cDNA was performed using the RT2 first strand synthesis kit (Qiagen) and the 96-well RT2 Profiler PCR Array plates (Qiagen, PAHS-027ZA) were prepared according to manufacturer's instructions. The assay was performed on three independent preparations of cells for each condition. The RT2 PCR Array datasets were processed using the SAB PCR Array Data Analysis Web portal (www.SABiosciences.com/pcrarraydataanalysis.php) with a boundary cutoff of 3-fold increase in expression.

Cell death assays. Cells were prepared as described in the RT-PCR section and treated identically to alter pHi. Three wells of each condition were trypsinized and mixed with Trypan blue for counting. Cells were counted using a hemocytometer and percent dead cells reported and normalized within each experiment to that observed with p53-WT at low pHi. Data analyzed from 4 experiments (Student's t-tests, unpaired, two-tailed, Holm-Sidak multiple comparisons correction).

pHi measurements. For each condition, triplicate wells were plated (2×10^4 per well; 24-well plate). Steady-state pHi was measured (*33*) under conditions outlined in *pHi control* sections. For each graph, data analyzed from three experiments (Student's t-tests, unpaired, two-tailed).

SUPPLEMENTARY MATERIAL INCLUDES
Supplementary Figures 1-5
Supplementary Methods: details on MD analysis, protein purification, and immunoblotting

REFERENCES

1. R. A. Cardone, V. Casavola, S. J. Reshkin, The role of disturbed pH dynamics and the Na+/H+ exchanger in metastasis. *Nat Rev Cancer* **5**, 786-795 (2005).

2. B. K. Grillo-Hill, C. Choi, M. Jimenez-Vidal, D. L. Barber, Increased H(+) efflux is sufficient to induce dysplasia and necessary for viability with oncogene expression. *Elife* **4**, (2015).

3. S. Harguindey, G. Orive, J. Luis Pedraz, A. Paradiso, S. J. Reshkin, The role of pH dynamics and the Na+/H+ antiporter in the etiopathogenesis and treatment of cancer. Two faces of the same coin--one single nature. *Biochim Biophys Acta* **1756**, 1-24 (2005).

4. B. A. Webb, M. Chimenti, M. P. Jacobson, D. L. Barber, Dysregulated pH: a perfect storm for cancer progression. *Nat Rev Cancer* **11**, 671-677 (2011).

5. R. J. Gillies, D. Verduzco, R. A. Gatenby, Evolutionary dynamics of carcinogenesis and why targeted therapy does not work. *Nat Rev Cancer* **12**, 487-493 (2012).

6. G. R. Bignell *et al.*, Signatures of mutation and selection in the cancer genome. *Nature* **463**, 893-898 (2010).

7. L. B. Alexandrov *et al.*, Signatures of mutational processes in human cancer. *Nature* **500**, 415-421 (2013).

8. H. Tan, J. Bao, X. Zhou, Genome-wide mutational spectra analysis reveals significant cancer-specific heterogeneity. *Sci Rep* **5**, 12566 (2015).

9. P. Anoosha, R. Sakthivel, M. Michael Gromiha, Exploring preferred amino acid mutations in cancer genes: Applications to identify potential drug targets. *Biochim Biophys Acta* **1862**, 155-165 (2016).

10. A. Schonichen, B. A. Webb, M. P. Jacobson, D. L. Barber, Considering protonation as a posttranslational modification regulating protein structure and function. *Annu Rev Biophys* **42**, 289-314 (2013).

11. S. A. Forbes *et al.*, COSMIC: mining complete cancer genomes in the Catalogue of Somatic Mutations in Cancer. *Nucleic Acids Res* **39**, D945-950 (2011).

12. N. Jura, Y. Shan, X. Cao, D. E. Shaw, J. Kuriyan, Structural analysis of the catalytically inactive kinase domain of the human EGF receptor 3. *Proc Natl Acad Sci U S A* **106**, 21608-21613 (2009).

13. X. Zhang, J. Gureasko, K. Shen, P. A. Cole, J. Kuriyan, An allosteric mechanism for activation of the kinase domain of epidermal growth factor receptor. *Cell* **125**, 1137-1149 (2006).

14. N. Jura *et al.*, Catalytic control in the EGF receptor and its connection to general kinase regulatory mechanisms. *Mol Cell* **42**, 9-22 (2011).

15. T. J. Lynch *et al.*, Activating mutations in the epidermal growth factor receptor underlying responsiveness of non-small-cell lung cancer to gefitinib. *N Engl J Med* **350**, 2129-2139 (2004).

16. C. H. Yun *et al.*, Structures of lung cancer-derived EGFR mutants and inhibitor complexes: mechanism of activation and insights into differential inhibitor sensitivity. *Cancer Cell* **11**, 217-227 (2007).

17. Y. Li, X. Li, W. Ma, Z. Dong, Conformational Transition Pathways of Epidermal Growth Factor Receptor Kinase Domain from Multiple Molecular Dynamics Simulations and Bayesian Clustering. *J Chem Theory Comput* **10**, 3503-3511 (2014).

18. A. Papakyriakou, D. Vourloumis, F. Tzortzatou-Stathopoulou, M. Karpusas, Conformational dynamics of the EGFR kinase domain reveals structural features involved in activation. *Proteins* **76**, 375-386 (2009).

19. M. Mustafa, A. Mirza, N. Kannan, Conformational regulation of the EGFR kinase core by the juxtamembrane and C-terminal tail: a molecular dynamics study. *Proteins* **79**, 99-114 (2011).

20. A. Dixit, G. M. Verkhivker, Hierarchical modeling of activation mechanisms in the ABL and EGFR kinase domains: thermodynamic and mechanistic catalysts of kinase activation by cancer mutations. *PLoS Comput Biol* **5**, e1000487 (2009).

21. Z. Ruan, N. Kannan, Mechanistic Insights into R776H Mediated Activation of Epidermal Growth Factor Receptor Kinase. *Biochemistry* **54**, 4216-4225 (2015).

22. C. L. McClendon, L. Hua, A. Barreiro, M. P. Jacobson, Comparing Conformational Ensembles Using the Kullback-Leibler Divergence Expansion. *J Chem Theory Comput* **8**, 2115-2126 (2012).

23. L. K. Putney, D. L. Barber, Na-H exchange-dependent increase in intracellular pH times G2/M entry and transition. *J Biol Chem* **278**, 44645-44649 (2003).

24. A. C. Joerger, A. R. Fersht, The tumor suppressor p53: from structures to drug discovery. *Cold Spring Harb Perspect Biol* **2**, a000919 (2010).

25. Y. Chen *et al.*, Structure of p53 binding to the BAX response element reveals DNA unwinding and compression to accommodate base-pair insertion. *Nucleic Acids Res* **41**, 8368-8376 (2013).

26. H. C. Ang, A. C. Joerger, S. Mayer, A. R. Fersht, Effects of common cancer mutations on stability and DNA binding of full-length p53 compared with isolated core domains. *J Biol Chem* **281**, 21934-21941 (2006).

27. M. Brazdova *et al.*, Preferential binding of hot spot mutant p53 proteins to supercoiled DNA in vitro and in cells. *PLoS One* **8**, e59567 (2013).

28. W. S. el-Deiry *et al.*, WAF1, a potential mediator of p53 tumor suppression. *Cell* **75**, 817-825 (1993).

29. S. P. Denker, D. C. Huang, J. Orlowski, H. Furthmayr, D. L. Barber, Direct binding of the Na--H exchanger NHE1 to ERM proteins regulates the cortical cytoskeleton and cell shape independently of H(+) translocation. *Mol Cell* **6**, 1425-1436 (2000).

30. A. Karydis, M. Jimenez-Vidal, S. P. Denker, D. L. Barber, Mislocalized scaffolding by the Na-H exchanger NHE1 dominantly inhibits fibronectin production and TGF-beta activation. *Mol Biol Cell* **20**, 2327-2336 (2009).

31. K. Aertgeerts *et al.*, Structural analysis of the mechanism of inhibition and allosteric activation of the kinase domain of HER2 protein. *J Biol Chem* **286**, 18756-18765 (2011).

32. M. P. Jacobson *et al.*, A hierarchical approach to all-atom protein loop prediction. *Proteins* **55**, 351-367 (2004).

33. C. H. Choi, B. A. Webb, M. S. Chimenti, M. P. Jacobson, D. L. Barber, pH sensing by FAK-His58 regulates focal adhesion remodeling. *J Cell Biol* **202**, 849-859 (2013).

ACKNOWLEDGEMENTS

The authors thank B. Vogelstein, K. Vousden, and N. Jura for sharing plasmids. We thank J. Roose for sharing the BRAF-V600E-inducible NIH-3T3 cell line and J. M. Bishop for sharing the MDA-MB-157 cell line. We also thank N. Jura for helpful discussions on EGFR. This work was supported by National Institutes of Health grants CA178706 to Diane L. Barber and Ryan D. Hernandez; CA197855 to Diane L. Barber, and HG007644 to Ryan D. Hernandez; and National Institutes of Health F32 grant CA177085 to Katharine A. White. M.P.J. is a

consultant to and stockholder of Schrodinger LLC, which distributes some of the software used in this work. **Author contributions**: D.L.B. conceived the hypothesis, which was developed in collaboration with K.A.W., R.D.H., and M.P.J. K.A.W directed collaborations and performed all biochemical and cell-based assays. D.L.B. performed pHi measurements. D.G.R. performed MD simulations and analyses. K.A.W. and D.G.R., performed data analysis. Z.A.S. and N.B.S. contributed valuable discussions of data and ideas. All authors contributed to writing the manuscript. Correspondence should be addressed to Diane Barber, diane.barber@ucsf.edu.

Figure Legends

Fig. 1. EGFR-R776H has pH-sensitive activity and downstream signaling, with increased activity at higher pHi. A) Structures of inactive (left, 3GT8) and active (right, 2GS6) wild-type (WT) EGFR. Arg776 shown in stick, αC helix in red, heteroatom distances (Å) noted in yellow. **B**) *in vitro* kinase activity of WT and EGFR-R776H (R776H) determined by [γ-^{32}P]-ATP incorporation into enzyme (autophosphorylation) or substrate peptide (substrate) at two pH values. Data normalized to autophosphorylation of WT at pH 6.8. Representative gel and autoradiograph in Fig. S1A. **C**) Representative immunoblots of lysates from quiescent MDA-MB-453 cells transfected with EGFR WT, R776H, or R776G at indicated pHi values with (+) or without (-) EGF (50 ng/mL; 5 min). Blots of total EGFR (EGFR), EGFR autophosphorylation (pY1173), AKT-pS473 (pAKT), ERK, and ERK1/2-pT202/Y204 (pERK). **D-F**) Quantification of pY1173 (D), pAKT (E), and pERK (F), in all cases normalized to amount of total EGFR present. Three replicate experiments were quantified in A, and four replicate experiments were quantified in D-F (mean ± SEM; * $p<0.05$, ** $p<0.01$, *** $p<0.001$).

Fig. 2. Protonation state of His776 alters EGFR αC helix conformations sampled in MD simulations. A) Jensen-Shannon divergence of protonated vs. neutral R776H highlights major differences localized on one end of the αC helix. **B**) αC helix conformational distribution for 300 ns molecular dynamics simulations defined by two angle measures (see Fig. S3A) that describe tilting and displacement of the helix relative to the active crystal structure. Circles denote the tilt and displacement of active (yellow) and inactive (black) crystal structures. See Fig. S3C for comparisons including R776G. **C**) Final snapshots of simulations for each EGFR construct: WT (left), neutral R776H (middle) and protonated R776H (right).

Fig. 3. EGFR-R776H has pH-sensitive proliferation and soft-agar transformation.

A) EGFR immunoblot of parental NIH-3T3 (3T3) cells and 3T3 cells stably expressing EGFR WT, R776H, or R776G. Calculated values shown for EGFR normalized to actin loading control. **B**) Experimentally changed pHi in 3T3 cell lines stably expressing EGFR WT, R776H, or R776G. Medium was supplemented with 5 mM NH_4Cl for 48 h (NH_4Cl) to raise pHi and 10 μM EIPA for 48 h (EIPA) to lower pHi. **C**) pHi-dependent proliferation of NIH-3T3 cells stably expressing EGFR WT, R776H, or R776G. Fold-increase in cell number normalized for each experiment to parental 3T3 at pHi 7.4. **D**) Representative images of soft-agar transformation assay for NIH-3T3 cells stably expressing EGFR WT, R776H, R776G, or BRAF-V600E. Cells were maintained for 15 days in complete medium or medium supplemented with 5 mM NH_4Cl; medium was replaced every 3 days. Cells were fixed and stained with crystal violet. **E**) Quantification of soft-agar transformation assays. ImageJ particle analyzer was used to count colonies >8 square pixels (see Methods). For B, C, and E at least three replicate experiments were quantified (mean ± SEM; * $p<0.05$, ** $p<0.01$, *** $p<0.001$).

Fig. 4. p53-R273H has decreased DNA binding at higher pHi. A) Structure of p53 (4HJE) with Arg273 and Arg175 in magenta stick **B**) Luciferase assay in PS120 E266I cells transiently transfected with p53 WT, R273H, R273L, or R175H at two pHi values (see Fig S4A for pHi measurements). Luciferase signal was normalized first to beta-galactosidase control and then within each experiment to WT at pHi 7.1. **C**) RT-PCR from etoposide-treated MDA-MB-157 cells stably expressing WT or p53-R273H at two pHi values (see Fig S4B for pHi measurements). Scatter plots of (2^-ΔC(t)) on log10 scale for wild-type (left) and R273H (right) at pHi 7.2 vs. pHi 7.6. Lines are identity (solid) and 3-fold boundaries (dotted). Indicated are transcripts that are more (red) or less (blue) abundant at pHi 7.2 relative to 7.6 (see Fig. S3 for

altered transcripts). **D**) Death assay. Cells were treated as in C and triplicate wells of each condition were trypsinized, mixed with trypan blue, and counted. Ratios of dead cells to total cells were calculated. For B, C, and D at least three replicate experiments were quantified (mean ± SEM; * $p<0.05$, *** $p<0.001$).

White, *et al.* Figure 1

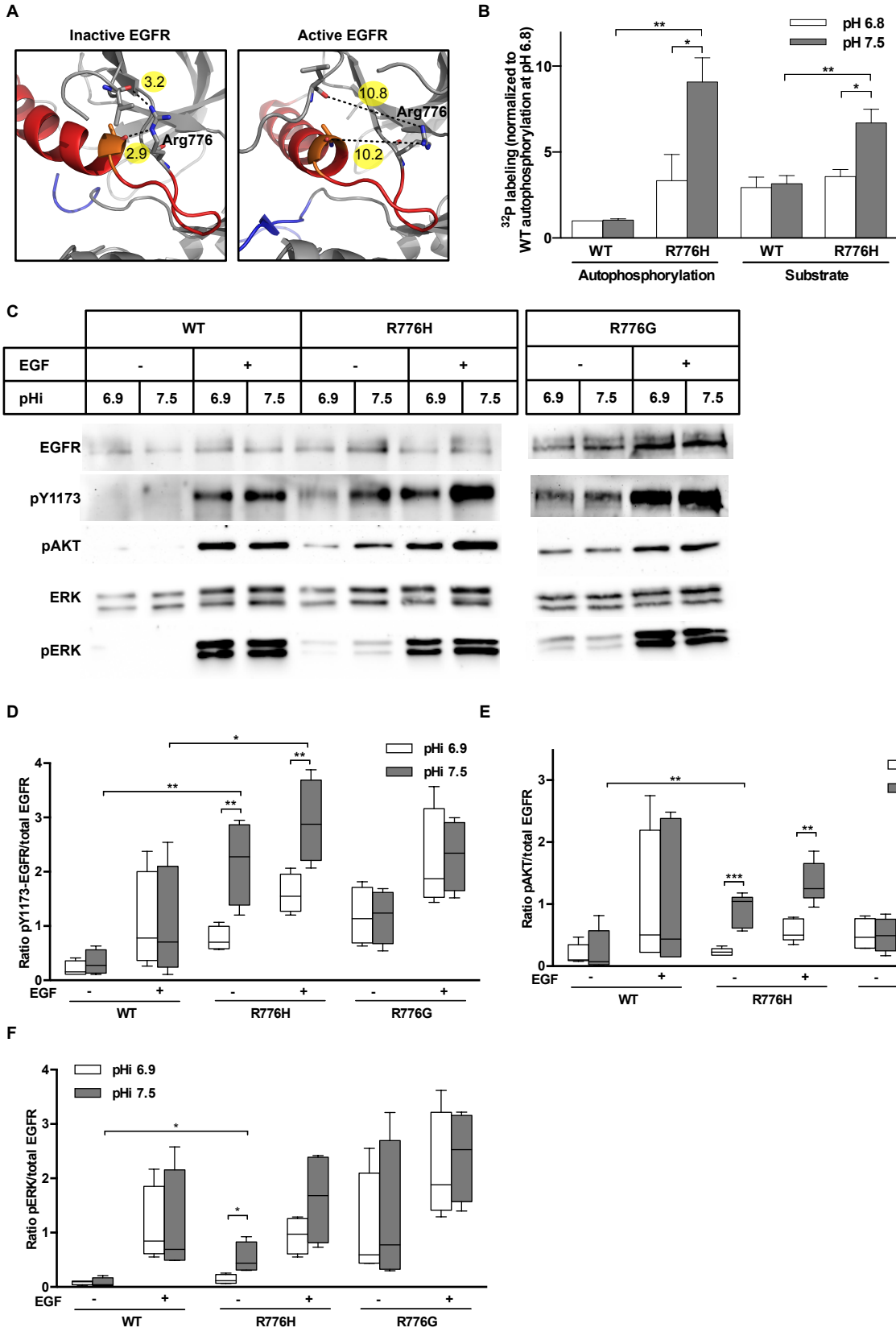

White, *et al.* Figure 2

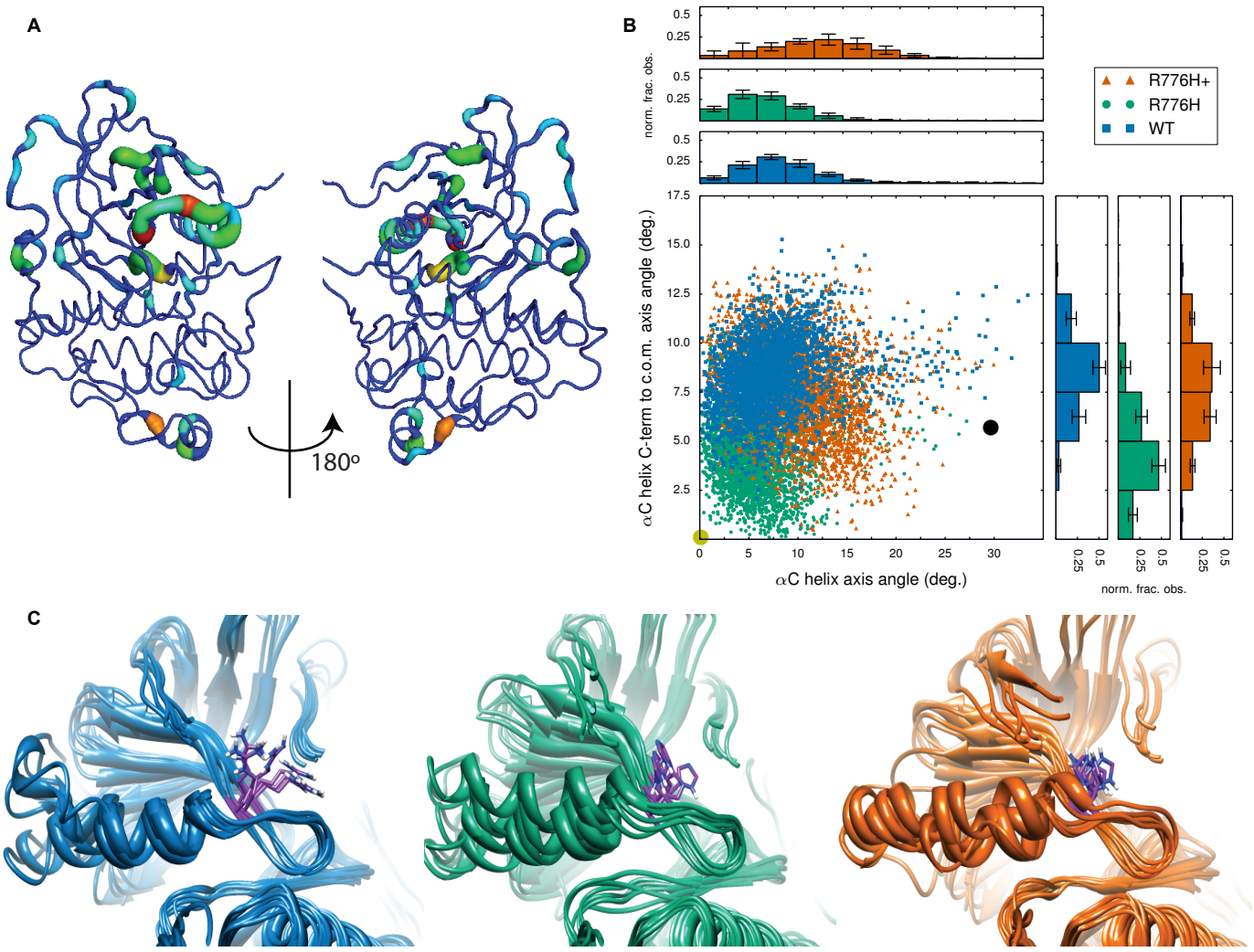

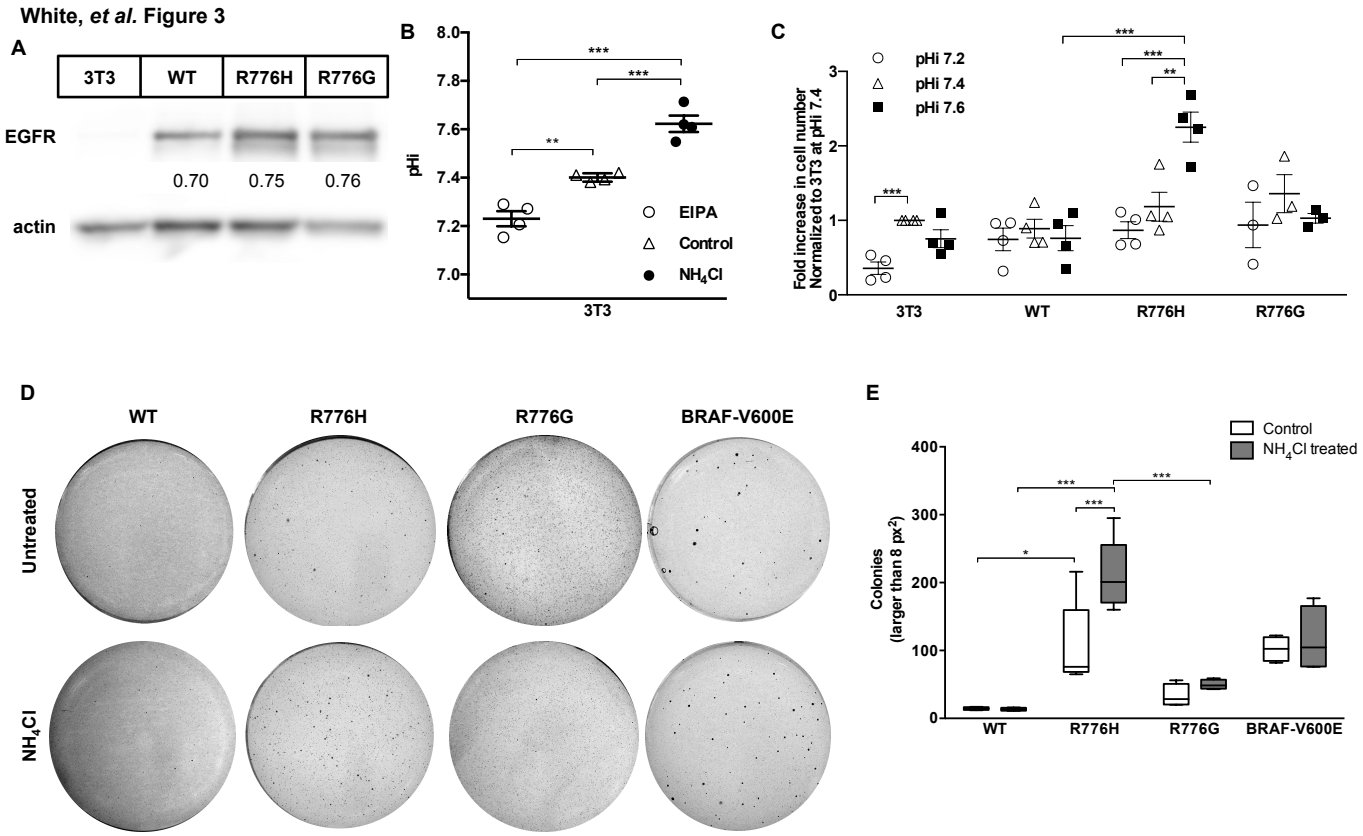
White, *et al.* Figure 3
A
3T3
WT
R776H
R776G
EGFR
0.70
0.75
0.76
actin
B
pHi
8.0
7.8
7.6
7.4
7.2
7.0
***
***
**
EIPA
Control
NH4Cl
3T3
C
Fold increase in cell number
Normalized to 3T3 at pHi 7.4
pHi 7.2
pHi 7.4
pHi 7.6
3
2
1
0
***
***
***
**
3T3
WT
R776H
R776G
D
WT
R776H
R776G
BRAF-V600E
Untreated
NH4Cl
E
Control
NH4Cl treated
Colonies
(larger than 8 px2)
400
300
200
100
0
*
***
***
***
WT
R776H
R776G
BRAF-V600E

White, *et al.* Figure 4

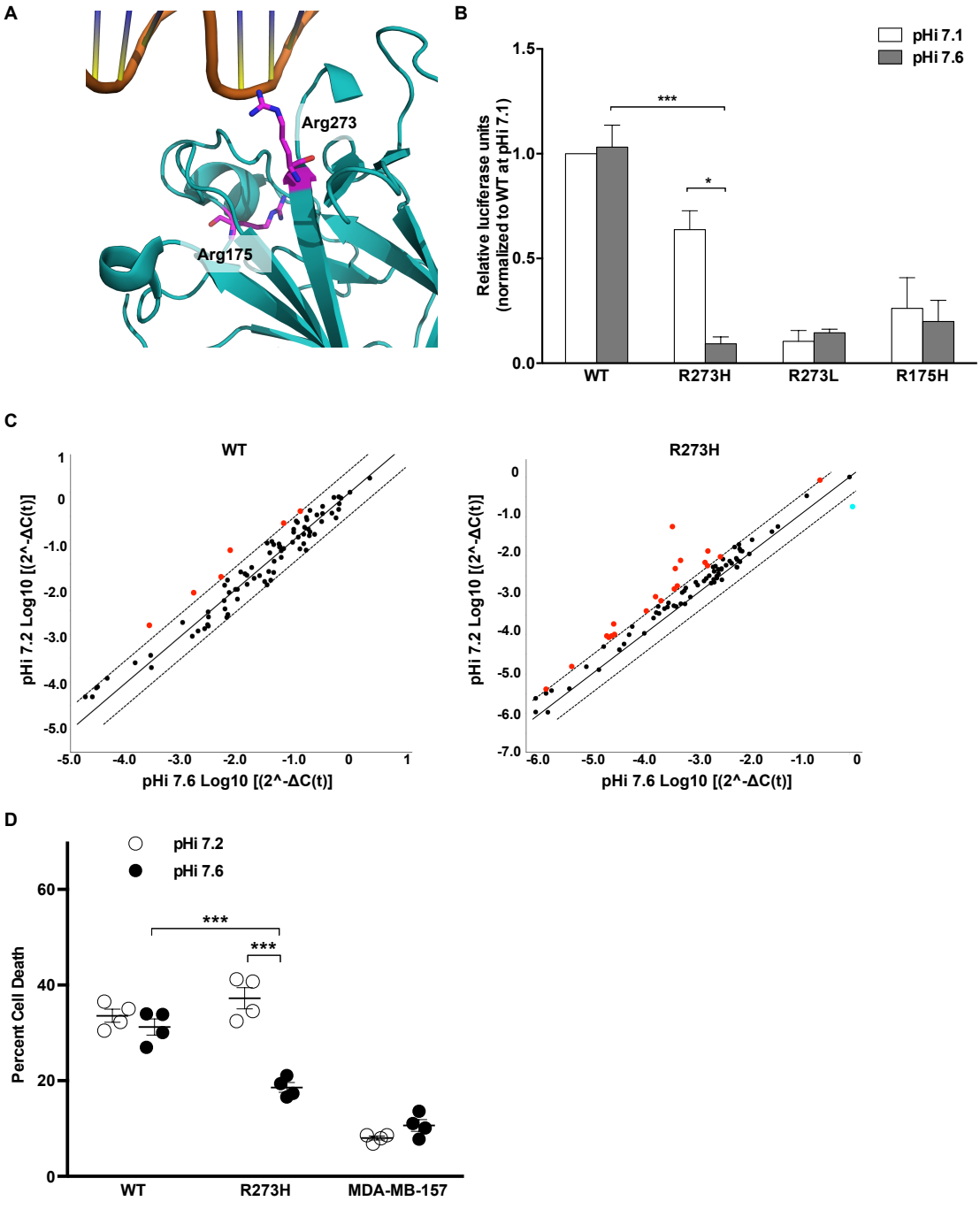

Supplementary Material includes:

Supplementary Figures 1-5
Supplementary Methods

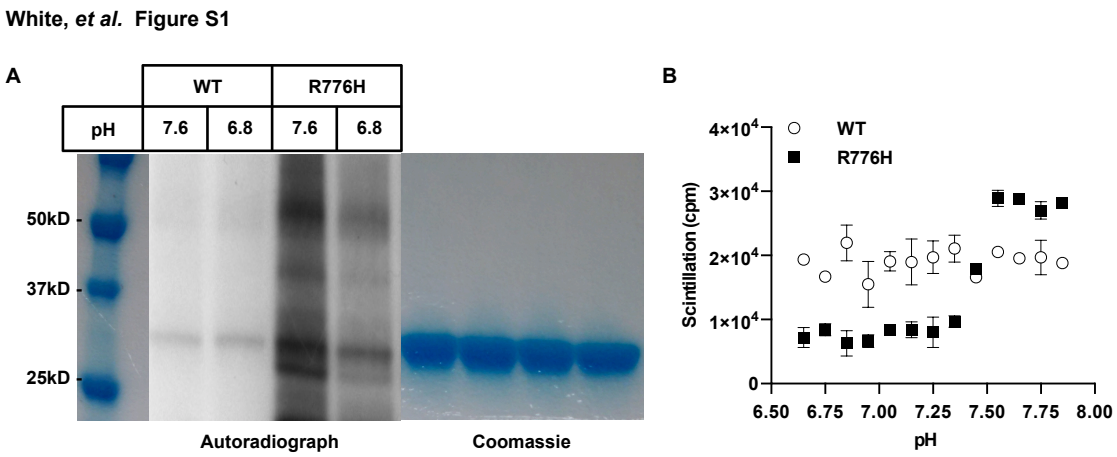

Figure S1. EGFR-R776H activity is pH sensitive *in vitro* and titrates with increasing pH. **A**) Coomassie-stained gel and autoradiograph of *in vitro* EGFR kinase assays with WT and EGFR-R776H. Enzyme autophosphorylation (~50 kDa) and phosphorylation of GST-fused substrate peptide (TAENAEYLRVAPQ) (~27 kDa). Quantification of triplicate experiments is shown in Figure 2B. **B**) *in vitro* kinase assays with WT and R776H performed at indicated pH values. Reactions were trapped on Whatman P-81 paper, washed, and total ^{32}P incorporation measured by scintillation counting (mean ± SD).

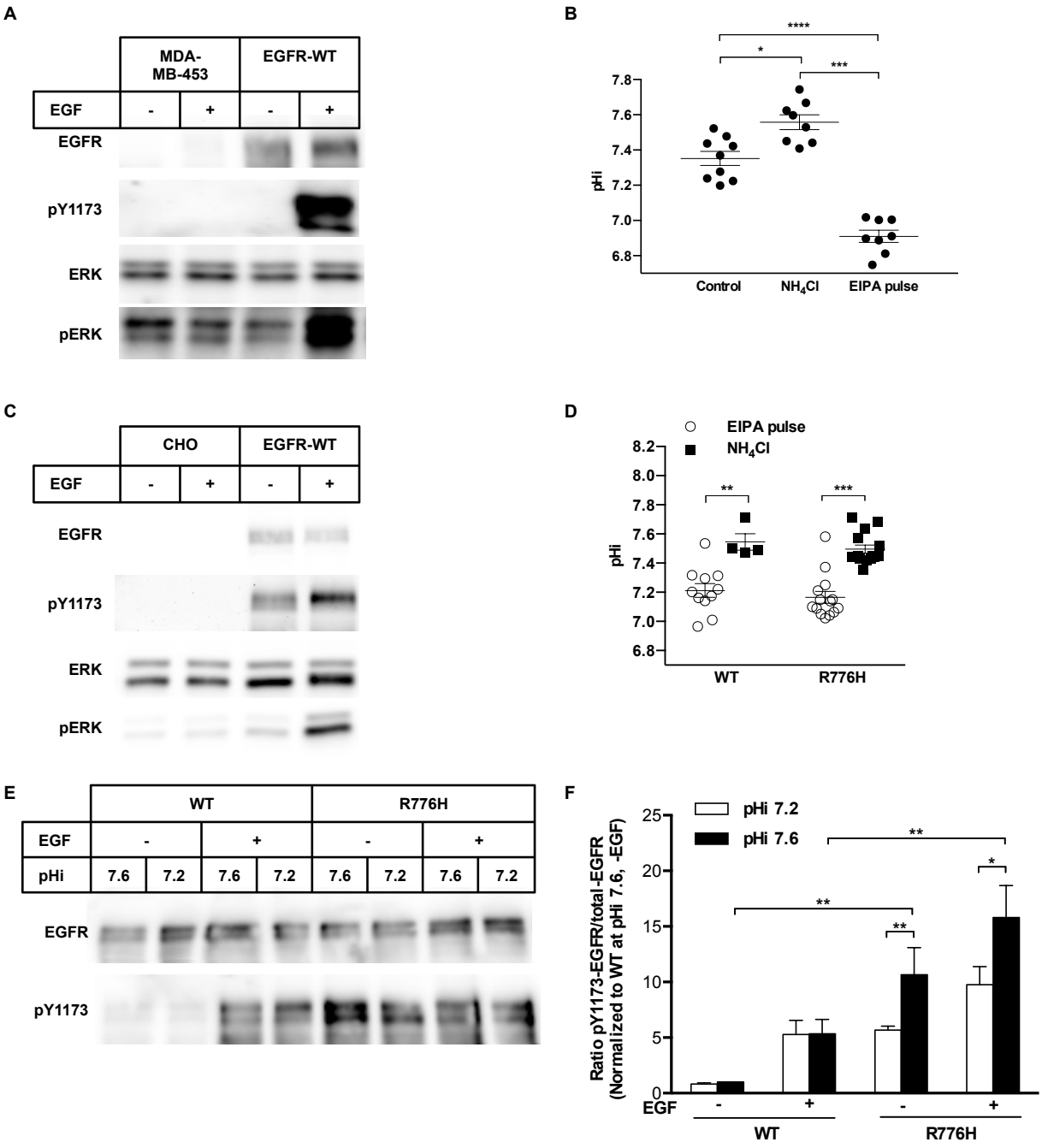

Figure S2. EGFR-R776H has pH-sensitive activity and downstream signaling, with increased activity at higher pHi. A) Immunoblot of lysates from quiescent MDA-MB-453 cells or transfected with EGFR-WT, with (+) and without (-) EGF (50 ng/mL; 5 min). Blots of EGFR, EGFR-pY1173, ERK, and ERK1/2-pT202/Y204 (pERK). **B**) Experimentally changed pHi in quiescent MDA-MB-453 cells. To increase pHi, cells incubated in serum free medium (SFM) with 15 mM NH_4Cl for 10 minutes (NH_4Cl). To decrease pHi, cells incubated in SFM containing 15 mM NH_4Cl for 10 minutes, then medium was replaced with SFM containing 1 μM EIPA for 5 minutes (EIPA pulse) (see Methods for details). **C**) Immunoblots of lysates from quiescent EGFR-null CHO cells untransfected (Parental) or transfected with EGFR WT. Conditions include with (+) and without (-) EGF (50 ng/mL; 5 min). Blots are shown for EGFR, EGFR-

pY1173, ERK and ERK1/2- pT202/Y204 (pERK). **D**) Experimentally changed pHi was achieved as in B) and measured. **E**) Representative immunoblots of lysates from quiescent CHO cells transfected with EGFR WT or R776H, at the indicated pHi values with (+) or without (-) EGF (50 ng/mL; 5 min). Blots shown for EGFR and EGFR-pY1173. **F**) Quantification of EGFR-pY1173 to total EGFR ratios, normalized to that observed with WT at pHi 7.6 in the absence of EGF. For B, D and F, at least three replicate experiments were quantified (mean ± SEM; * $p<0.05$, ** $p<0.01$, *** $p<0.001$).

White, *et al*. Figure S3

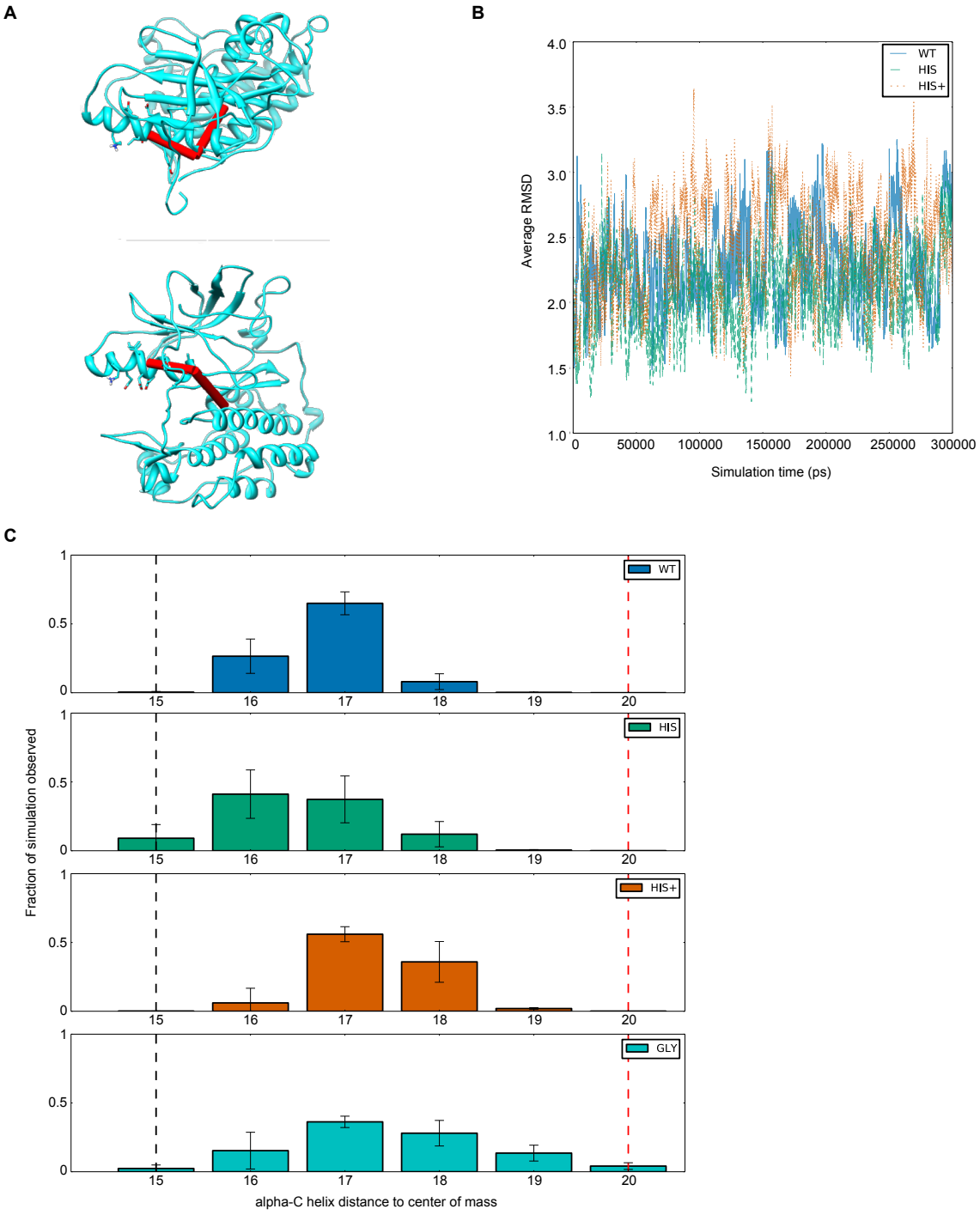

Figure S3. EGFR MD simulations metrics for analysis and quality control. A) Illustration of the vectors that define the axes used to characterize the conformation of the αC helix. Top view (top) and back view (bottom). **B**) Running average RMSD of the molecular dynamics trajectories generated for the analysis. **C**) Histograms of the distance between the center of mass of the αC helix and the center of mass of the system. The R776G mutant is more flexible than both WT and R776H and primarily adopts intermediate conformations between active-like and inactive-like.

White, *et al.* Figure S4

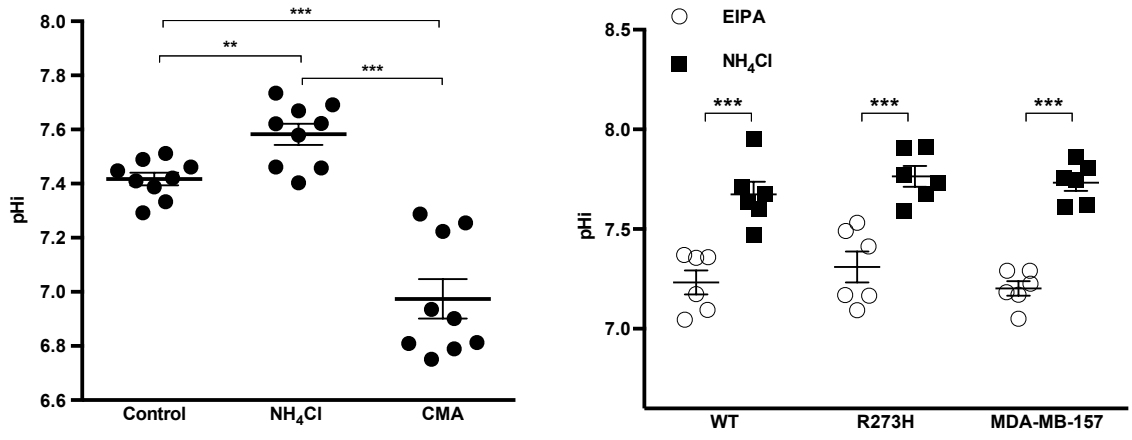

Figure S4. pHi control for p53 assays A) The pHi in PS120-E266I cells was increased by supplementing medium with 5 mM NH_4Cl for 48 h (NH_4Cl) and decreased by supplementing medium with 0.1 μM concanamycin A (CMA), an inhibitor of vacuolar-type H^+/ATPase (V-ATPase), for 48 h. Three replicate experiments were quantified (mean ± SEM; ** $p < 0.01$, *** $p< 0.001$). **B**) The pHi in MDA-MB-157 cells was increased by supplementing medium with 5 mM NH_4Cl for 48 h (NH_4Cl) and decreased by supplementing medium with 10 μM EIPA for 48 h. Three replicate

White, *et al.* Figure S5

R273H: Genes with altered transcript abundance at low pHi			
Gene	**Fold Change at pHi 7.2**	**Function**	**Description**
APAF1	4.43	Apoptotic gene	Apoptotic peptidase activating factor 1
ATM	7.12	DNA repair, negative regulator of cell cycle	Ataxia telangiectasia mutated
BIRC5	5.34	anti-apoptosis	Baculoviral IAP repeat containing 5
BRCA1	14.77	DNA repair gene	Breast cancer 1, early onset
BTG2	3.81	Negative regulator of cell growth	BTG family, member 2
CASP2	11.22	anti-apoptosis	Caspase 2, apoptosis-related cysteine peptidase
CDKN2A	7.55	Cell cycle arrest	Cyclin-dependent kinase inhibitor 2A (melanoma, p16, inhibits CDK4)
CHEK1	151.69	Cell cycle arrest	CHK1 checkpoint homolog (S. pombe)
EGR1	4.68	Growth	Early growth response 1
EI24	3.01	Inducer of apoptosis	Etoposide induced 2.4 mRNA
FADD	4.32	Inducer of apoptosis	Fas (TNFRSF6)-associated via death domain
FAS	3.90	Inducer of apoptosis	Fas (TNF receptor superfamily, member 6)
IL6	3.69	Regulator of cell growth	Interleukin 6 (interferon, beta 2)
NF1	3.16	Negative regulator of cell cycle	Neurofibromin 1
NFKB1	3.32	anti-apoptosis	Nuclear factor of kappa light polypeptide gene enhancer in B-cells 1
PPM1D	3.76	Negative regulator of cell cycle	Protein phosphatase, Mg2+/Mn2+ dependent, 1D
PRC1	3.53	Cell cycle gene	Protein regulator of cytokinesis 1
TNF	3.22	anti-apoptosis	Tumor necrosis factor
TNFRSF10B	3.53	Inducer of apoptosis	Tumor necrosis factor receptor superfamily, member 10b
PTTG1	-6.51	Growth	Pituitary tumor-transforming 1

WT: Genes with altered transcript abundance at low pHi			
Gene	**Fold Change at pHi 7.2**	**Function**	**Description**
MSH2	3.11	DNA repair, negative regulator of cell cycle	MutS homolog 2, colon cancer, nonpolyposis type 1 (E. coli)
PTEN	3.42	Negative regulator of cell cycle	Phosphatase and tensin homolog
RB1	4.84	Negative regulator of cell cycle	Retinoblastoma 1
SESN2	3.49	Cell cycle arrest	Sestrin 2
SIRT1	8.61	Apoptosis gene	Sirtuin 1
TP73	6.20	Inducer of apoptosis	Tumor protein p73

Figure S5. pH-dependent transcriptional profiles. pH-sensitive transcriptional targets for p53-R273H (top) and WT (bottom). Listed in red are all genes with transcript levels that are >3-fold higher at pHi 7.2 relative to pHi 7.6. Listed in blue are genes with transcript levels that are >3-fold lower at pHi 7.2 relative to pHi 7.6. Three replicate experiments were quantified (mean ± SEM; *** $p < 0.001$).

Supplementary Methods

Cloning and expression *EGFR substrate peptide: pGEX6P-GST-Peptide* Complementary oligos for EGFR substrate peptide TAENAEYLRVAPQ (1) flanked by EcoRI and XhoI sites were ordered, annealed, and ligated into pGEX6P digested with EcoRI and XhoI.

FP:**AATTC**CCACCGCGGAAAACGCGGAATATCTGCGCGTGGCGCCGCAGTGA**C**

RP:**TCGAG**TCACTGCGGCGCCACGCGCAGATATTCCGCGTTTTCCGCGGTGG**G**

Construct was transformed into and expressed in BL21-DE3 *E. coli*. Cells were grown in LB + 100 μg/mL ampicillin (37 °C, with shaking) until OD_{600}= 0.5 and induced (1 mM IPTG, 12 h, room temperature, with shaking). Cells were pelleted (6,000×g; 10 min at 4 °C), resuspended in binding buffer (25 mM Tris pH 7.5, 150 mM NaCl, 1 mM EDTA, protease inhibitor cocktail (Roche)), and lysed by passing 6 times through a microfluidizer (Microfluidics; M110-S), cooling lysate between passages. Clarified supernatant (14,000×g; 10 min at 4 °C) was loaded onto to a pre-equilibrated glutathione-agarose column (Thermo Fisher), washed with 20 column volumes binding buffer, and the protein was eluted in binding buffer with 15 mM reduced glutathione, pH 8.0. GST-Peptide was concentrated and dialyzed into storage buffer: 10 mM Tris, 50 mM NaCl, 1 mM DTT, 5% glycerol, pH 7.5. Aliquots were flash frozen in liquid nitrogen and stored at -80 °C.

EGFR kinase: pFASTBAC-EGFR(645-998) (plasmid gift of N. Jura Lab) was mutated (Quickchange; Stratagene) to create pFASTBAC-EGFR-R776H. Recombinant baculovirus production, expression and purification of both wild-type and mutant EGFR (residues 645-998) from Hi5 insect cells were performed as described (1). Proteins were concentrated to 5–10 mg/mL and dialyzed into storage buffer: 20 mM Tris, 50 mM NaCl, 2 mM DTT, 2 mM TCEP, and 10% glycerol, pH 8.0. Aliquots were flash-frozen in liquid nitrogen and stored at -80 °C.

EGFR *in vitro* kinase assays. Reactions were assembled with 1 μM purified EGFR and 1 mM ATP with 25,000 cpm mol^{-1} of [γ-^{32}P]-ATP in kinase buffer (50 mM HEPES, 10 mM $MgCl_2$, 100 μM DTT, at pH 6.8 or 7.5) and pre-incubated at 25 °C for 10 min. After pre-incubation, 3 μM GST-substrate peptide (TAENAEYLRVAPQ (1)) fusion (C_f) was added, reactions incubated at 25 °C for 10 min, then quenched (EDTA; 25 mM C_f). Reactions were mixed with Laemmli buffer, boiled, run on 10% SDS-PAGE gels, and dried using a gel dryer (Biorad, Model 853). Autoradiograph film (Denville Hyblot CL, E3018) was exposed overnight at -20 °C. For pH titration, reactions were performed as above in kinase buffers prepared at a range of pH values. Quenched reactions were divided in half, captured on duplicate Whatman P-81 disks, and washed as described (2). [^{32}P] incorporation was measured by scintillation counting (Packard; TriCarb 2100TR) and averaged. Using ImageJ software, background-subtracted autoradiography intensities were determined and normalized within each experiment to autophosphorylation observed with WT-EGFR at pH 6.8. Data analyzed from three experiments (Student's t-tests, unpaired, two-tailed, Holm-Sidak multiple comparisons correction).

Cell culture MDA-MB-453 (ATCC) and MDA-MB-157 (J. M. Bishop Lab): Leibovitz L15 with 15% FBS, grown in atmospheric conditions at 37 °C. CHO (ATCC): MEM-alpha with 10% FBS, grown in 5% CO_2 at 37 °C. NIH-3T3 (J. Roose Lab): DMEM (GIBCO) with 10% FBS, grown in 5% CO_2 at 37 °C. PS120-E266I: DMEM (GIBCO) with 5% FBS, grown in 5% CO_2 at 37 °C.

Western Blotting and quantification. For each sample, 10 μg of total protein per lane (Bradford assay) was prepared (add Laemmli loading buffer, boiled) and loaded on duplicate 10% SDS-PAGE gels. Proteins were transferred to 0.45 μm PVDF membranes (Immobilon)

(50V, 2.5 h, on ice). Membranes were blocked in 5% milk/TBST (0.1% Tween in TBS) for 1 h at room temperature and then divided for blotting based on pre-stained protein ladder. 100+ kDa for total EGFR and EGFR-pY1173 (Cell Signaling 2232 and 4407; 1:1,000 in 5% BSA/TBST); 50–100 kDa for AKT-pS473 (Cell Signaling 9271; 1:1,000 in 5% milk/TBST); 10–50kDa for total ERK and ERK1/2- pT202/Y204 (Santa Cruz sc93, Cell Signaling 4377; 1:5,000 in 5% milk/TBST). Where indicated, actin was blotted (Millipore MAB1501; 1:10,000 in 5% milk/TBST). Primary antibodies were incubated overnight (4 °C, with shaking). Membranes were washed (3×5 min, TBST) with shaking. Secondary anti-mouse and anti-rabbit HRP antibodies (Biorad 1706515 and 1706516; 1:10,000 in 5% milk/TBST) were incubated for 1 h (room temperature, with shaking). Membranes were washed with shaking (3×5 min, TBST), developed (Supersignal West Femto; Pierce), and visualized (Alpha Innotech FluorChem Q). Using ImageJ software, background-subtracted densitometries for phospho-antibodies (EGFR-pY1173, AKT-pS473, or ERK1/2-pT202/Y204) were normalized to background-subtracted densitometries for total EGFR for each condition. Data from 3–4 experiments were analyzed (Student's t-tests, unpaired, two-tailed, Holm-Sidak multiple comparisons correction).

EGFR stable cell lines NIH-3T3 cells were transfected with pcDNA3-EGFR-WT, -R776G or -R776H (3.5 mm dish; Lipofectamine 2000, Invitrogen). 24 h post-transfection, cells were trypsinized and replated for selection (10 cm dish; 800 μg/mL zeocin, Invitrogen). When visible, individual colonies were isolated (cloning cylinders, Corning), EGFR expression was analyzed, and clones with similar expression levels propagated.

Molecular dynamics analysis. Convergence of the simulations was confirmed by RMSD plots. For each trajectory, the structures were aligned to a reference structure (active, 2GS6). To

characterize the conformation of the αC helix, we calculated the angle of the axis of the αC helix (resids 757-761 amide nitrogens center of mass to resids 764-768 amide nitrogens center of mass) and the angle of the axis defined by the vector from the αC helix center of mass to the center of mass of the full tyrosine kinase domain to the corresponding axes in the active crystal structure. Additionally, we calculated the distance between the center of mass of the αC helix (resids 756-767) to the center of mass of the tyrosine kinase. Conformational ensembles from molecular dynamic simulations were compared using the Jensen-Shannon divergence, which is a measure of dissimilarity between probability distributions. A discrete distribution of sampled torsion angles for each dihedral angle in the system is created for trajectories at each condition (WT, R776H protonated and neutral). These distribution are then compared using the JS divergence:

$$D_{KL}(P\|Q) = \sum_i P(i) \ln \frac{P(i)}{Q(i)}$$

$$D_{JS}(P\|Q) = \frac{1}{2} D_{KL}(P\|M) + \frac{1}{2} D_{KL}(Q\|M)$$

where $M = \frac{1}{2}(P+Q)$

With the JS divergence we can quantify the degree of dissimilarity between two dihedral angle distributions simulated under different conditions. Our calculations take into consideration sample variability using a statistical bootstrap approach with the full 6 independent simulations as reference (3).

Supplementary Methods References

1. Zhang X, Gureasko J, Shen K, Cole PA, & Kuriyan J (2006) An allosteric mechanism for activation of the kinase domain of epidermal growth factor receptor. *Cell* 125(6):1137-1149.
2. Barker SC*, et al.* (1995) Characterization of pp60c-src tyrosine kinase activities using a continuous assay: autoactivation of the enzyme is an intermolecular autophosphorylation process. *Biochemistry* 34(45):14843-14851.

3. McClendon CL, Hua L, Barreiro A, & Jacobson MP (2012) Comparing Conformational Ensembles Using the Kullback-Leibler Divergence Expansion. *J Chem Theory Comput* 8(6):2115-2126.